Postprint of: Ryżyńska Z., Klimczuk T., Winiarski M., Single crystal growth and physical properties of MCo_2Al_9 (M= Sr, Ba), JOURNAL OF SOLID STATE CHEMISTRY, Vol. 289 (2020), 121509, DOI: 10.1016/j.jssc.2020.121509

Single crystal growth and physical properties of MCo_2Al_9 (M= Sr, Ba)

Zuzanna Ryżyńska*, Tomasz Klimczuk, Michał J. Winiarski†

Faculty of Applied Physics and Mathematics, and Advanced Materials Centre, Gdansk University of Technology, Narutowicza 11/12, 80-233 Gdansk, Poland

* zuzanna.sobczak@pg.edu.pl

† michal.winiarski@pg.edu.pl

Single crystals of $SrCo_2Al$ and $BaCo_2Al_9$ were grown using a self-flux method. A LeBail analysis of the powder X-ray diffraction patterns show that both compounds crystallize in a hexagonal (*P6/mmm*) crystal structure with lattice parameters: a = 7.8995(1) Å, c = 3.9159(1) Å for $SrCo_2Al_9$, and a = 7.9162(2) Å, c = 3.9702(1) Å for $BaCo_2Al_9$ aluminide. The low temperature analysis of the heat capacity measurements give a Sommerfeld coefficient γ = 4.99(6) mJ mol^{-1} K^{-2} for $SrCo_2Al_9$ and almost twice larger γ = 7.94(9) mJ mol^{-1} K^{-2} for $BaCo_2Al_9$. Resistivity measurements show metallic-like behavior, with reasonably large residual resistivity ratio RRR = 6 and 10 for $SrCo_2Al_9$ and $BaCo_2Al_9$, respectively. Neither heat capacity nor resistivity measurements reveal any phase transition down to 1.8 K.

I Introduction

Aluminum rich polar intermetallics show a variety of structural types that can often be conveniently described as networks of interconnected Al endohedral clusters. Examples of particularly large structural families include the cubic $CeCr_2Al_{20}$ [1,2], tetragonal $CaCr_2Al_{10}$ [3,4], and hexagonal $Ho_6Mo_4Al_{43}$ [1]. The three groups have been a subject of an extensive research effort, due to their compositional versatility leading to a diversity of physical phenomena observed, including superconductivity [5–8], heavy fermion ground states [9–11], and magnetic order [1,10,12–14]. In a recent study a correlation between the occurrence of superconductivity and the valence electron count was observed in the group of gallide endohedral cluster compounds [15].

The hexagonal $BaFe_2Al_9$ family is much smaller, with 10 compounds reported in the Inorganic Crystal Structure Database, 7 of which being aluminides, that share the structural motif of interconnected endohedral transition metal-centered Al clusters stabilized by electron transfer from an electropositive atom (alkali, alkaline earth or rare earth metals). In all the known aluminide $BaFe_2Al_9$-type compounds the Ba position is occupied by a divalent metal (Ca, Sr, Ba, or Eu) and Fe position by Co, Fe or Ni [16,17], while the indide analogues were also reported with K and Ir occupying the Ba and Fe positions, respectively [18,19].

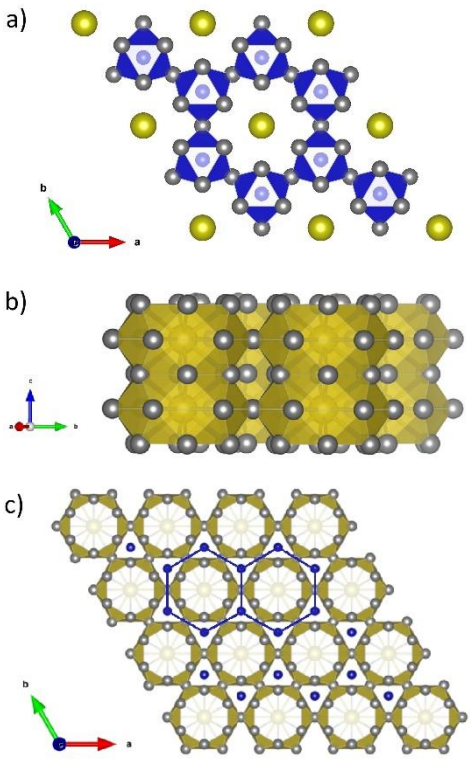

Fig. 1. Crystal structure of $BaFe_2Al_9$-type, where Ba, Fe and Al are represented by yellow, blue and grey balls respectively. a) clusters of Al atoms around Fe, b) clusters of Al around Ba atoms, c) Kagome structure of Al atoms and

honeycomb network of transition metal atoms. Images rendered using VESTA [20].

The structure of $BaFe_2Al_9$ can be understood as a network of $FeAl_9$ clusters sharing vertices (Al1) in the *ab* plane and triangular faces (formed by Al2) along the *c* direction (Fig. 1a). The voids of the hexagonal framework are occupied by Ba atoms which are coordinated by 18 Al atoms (12 x Al2 and 6 x Al1). These $BaAl_{18}$ polyhedra share only vertices (Al1) (see Fig. 1c).
As pointed out by Tremel and Hoffman [21], the "cluster analysis" of solid state compounds is just one of the several ways one can describe their structure. The $BaFe_2Al_9$ structure type can be thus viewed as an interweaving kagomé lattice of Al1 atoms, honeycomb network of transition metal atoms, and a triangular net of Ba within one plane, separated by honeycomb layer of Al2 atoms (Fig. 1c).
While the structure of $SrCo_2Al_9$ and $BaCo_2Al_9$ was described by Turban and Schäfer [16], in the literature, there are no reports of their physical properties. In this study we report single-crystal growth and physical characterization of the above mentioned compounds.

II Materials and Methods

Single crystals of $SrCo_2Al_9$ and $BaCo_2Al_9$ were synthesized using self-flux method. Strontium (Alfa Aesar, 99%) or barium (Alfa Aesar, 99.2%) pieces were put together with cobalt scraps (Alfa Aesar, 99.9+%) and aluminum slug (Alfa Aesar, 99.999%) in an alumina crucible at the atomic ratio of 1:2:40 (M:Co:Al). A frit-disc and a second crucible were used for flux separation as in [22]. The set was put in a quartz tube, evacuated and backfilled with Ar to dilute the Al vapor attacking the tube walls.

The ampoules were placed in a box furnace, heated to 1000°C, held for 2 hours and then slowly cooled (2°C/h) to 770°C. At this temperature the ampoules were centrifuged to separate crystals from the flux. The obtained crystals have cuboidal-like shape, are about 2 mm long, about 0.2 mm wide and thick and have shiny, silver color.

The phase purity and composition of the crystals was checked by powder x-ray diffraction (pXRD) using Bruker D2 Phaser 2nd generation diffractometer with Cu-*Kα* radiation and a LynxEye XE-T detector. Several crystals were fine ground using an agate mortar and pestle. The pXRD patterns were analyzed on the basis of LeBail refinement [23] with the PANalytical HighScore software.

Heat capacity and resistivity measurements were performed using a Quantum Design Physical Property Measurement System (PPMS). For specific heat the standard relaxation method was used. The two τ time-relaxation method was used to measure the specific heat. For electrical transport measurements, four 50 μm diameter platinum wire leads were attached to the crystal surface using a silver epoxy (Epo-Tek H20E). The measurements were carried out in the temperature range of 300 – 1.8 K.

Electronic structure calculations were performed by means of the Density Functional Theory (DFT) using the Quantum Espresso software package [24] employing the Perdew-Burke-Ernzerhof Generalized Gradient Approximation [25] of exchange-correlation potential. Rappe-Rabe-Kaxiras-Joannopoulos ultrasoft pseudopotentials [26] were used in their scalar- and fully-relativistic forms. Density of states integrations within the irreducible wedge of the primitive Brillouin zone were completed on a 10x10x16 *k*-point mesh. Kinetic energy cutoff for charge density and wavefunctions was set to 60 eV and 500 eV, respectively. Experimental crystal structures were relaxed using the Broyden–Fletcher–Goldfarb–Shanno (BFGS) algorithm.

III Results

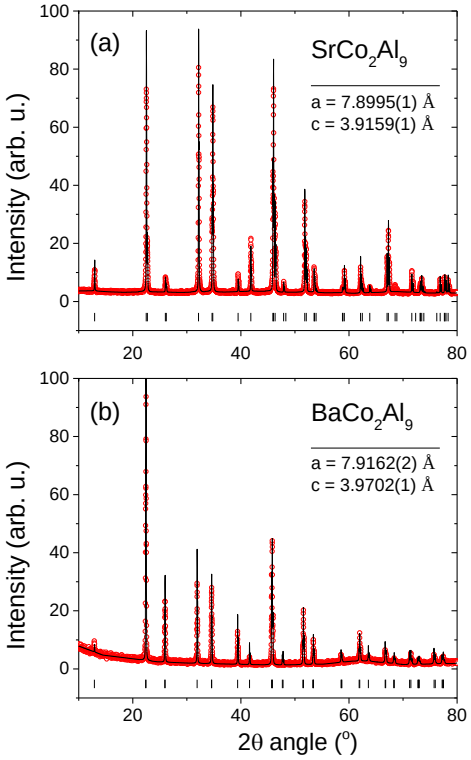

Figure 2 The X-ray powder diffraction characterization of crushed MCo_2Al_9 crystals (M=Sr, Ba). Red dots mark observed data and black solid line is the profile calculated with LeBail refinement. Black ticks mark Bragg positions of MCo_2Al_9.

Room temperature pXRD scans were performed in order to determine the composition and phase purity of the crystals. The results are presented in Fig. 2. All of the observed reflections are indexed to the hexagonal *P6*/*mmm* unit cell of $BaFe_2Al_9$ type.

LeBail refinement represented by black solid line in Fig. 2 gave the lattice parameters for $SrCo_2Al_9$: a = 7.8995(1) Å, c = 3.9159(1) Å, and for $BaCo_2Al_9$: a = 7.9162(1) Å, c = 3.9702(1) Å, which are in good agreement with the values reported previously [16,17]. Crystal structure parameters obtained from the LeBail refinements of the data in comparison with information from literature are presented in Tab. 1.

Tab. 1 Crystallographic data for MCo_2Al_9 crystals (M=Sr, Ba). Cell parameters and atomic positions obtained from the LeBail refinement are compared with the values reported previously [16,17].

MCo_2Al_9 (M=Sr, Ba)				
Space group	*P6*/*mmm* (# 191)			
Pearson symbol	hP12			
	$SrCo_2Al_9$		**$BaCo_2Al_9$**	
Cell parameters (Å)	This work	Ref. [16]	This work	Ref. [16]
a =	7.8995(1)	7.91	7.9162(1)	8.04
c =	3.9159(1)	3.96	3.9702(1)	3.89
Cell volume (Å^3)	211.601(3)		215.34(2)	
Molar weight (g/mol)	448.32		498.03	
Density (calculated) (g/cm^3)	5.08		4.13	

The main panels of Fig. 3 show the overall temperature dependence of the specific heat for a) $SrCo_2Al_9$ and b) $BaCo_2Al_9$. At room temperature, C_p is close to the expected by the Dulong-Petit law value 3nR ~ 300 J mol^{-1} K^{-1}, where n is the number of atoms per f.u. (n = 12) and R is gas constant (R = 8.31 J mol^{-1} K^{-1}). The solid red line through the data points denotes a fit to a combined model that includes electronic heat capacity (C_{el}) and phonon contribution (C_D and C_E) to the total C_p.

$$C_p = C_{el} + k \cdot C_D + (1-k) \cdot C_E,$$

where k is the weight of the Debye part. The electronic heat capacity is equal to:

$$C_{el} = \gamma T\left(1 - \frac{3\pi^2}{10}\left(\frac{T}{T_F}\right)^2\right),$$

where T_F is Fermi temperature and $T_F = E_F/k_B$. k_B is the Boltzmann constant ($k_B = 1.38 \cdot 10^{-23}$ J K^{-1}) and γ is the Sommerfeld coefficient. For metals the value of T_F is usually of the order of 10^4-10^5 K [27], so even at the highest temperatures we measured (~300 K) the expression can be simplified to:

$$C_{el} = \gamma T.$$

Debye (C_D) and Einstein (C_E) contributions to C_p are described by equations:

$$C_D = 9nR\left(\frac{T}{\Theta_D}\right)^3 \int_0^{\Theta_D/T} \frac{x^4 e^x}{(e^x-1)^2} dx,$$

and

$$C_E = 3nR\left(\frac{\Theta_E}{T}\right)^2 e^{\frac{\Theta_E}{T}} \left(e^{\frac{\Theta_E}{T}} - 1\right)^{-2},$$

where Θ_D and Θ_E denote characteristic Debye and Einstein temperatures.

The Debye temperatures estimated from the fits are equal to 443(2) K and 398(2) K, the Einstein temperatures are 99(4) K and 82(7) K, and the weight k = 0.93 and 0.97, for $SrCo_2Al_9$ and $BaCo_2Al_9$, respectively. It is clear that the Debye modes are dominant for both compounds. This distinguishes the two compounds from the cage intermetallics such as MT_2Al_{20} (M – rare earth metals and actinides, T – transition metals), where significant Einstein contributions were attributed to the vibrations of the electropositive atom in an oversized Al cage [7,8,28-33]. In $SrCo_2Al_9$ and $BaCo_2Al_9$, the movement of the encaged Sr/Ba atom is thus likely more strongly coupled to the cage, resulting in a Debye-type contribution to the heat capacity.

In the analysis we fixed the Sommerfeld parameter (γ) as obtained from a low temperature fit shown in the insets of Fig. 3. At sufficiently low temperatures (typically $T < \Theta_D/50$), the C_p can be described as

$C_p = \gamma T + \beta T^3$. Plotting C_p/T versus T^2, and using a linear fit, we got γ = 4.99(6) mJ mol^{-1} K^{-2} for $SrCo_2Al_9$ and 7.94(9) mJ mol^{-1} K^{-2} for $BaCo_2Al_9$. The second parameter, β, is related to the Debye temperature through $\Theta_D = \sqrt[3]{\frac{12\pi^4 nR}{5\beta}}$, where n is the number of atoms per formula unit (here n = 12). Taking β values from the fit, the estimated Debye temperatures are 436(2) K and 474(4) K, for $SrCo_2Al_9$ and $BaCo_2Al_9$, respectively. For $SrCo_2Al_9$ obtained Debye temperature is in a very good agreement with a value estimated from the whole temperature range fit. While the two methods of estimating the Debye temperature (low-temperature and whole-range fits) yield consistent results in case of $SrCo_2Al_9$, a discrepancy is seen in case of $BaCo_2Al_9$. This may reflect the details of the phonon structure of the two compounds, with $SrCo_2Al_9$ being described better by a single Debye oscillator model due to lower mass differences between the constituent elements.

In order to obtain Einstein temperature we plotted temperature dependence of $C_{lattice}/T^3$ (shown in Fig. 4), where $C_{lattice}$ is a lattice (phonon) contribution to the heat capacity and was calculated by subtracting $C_{el} = \gamma T$ from the total signal C_p. It can be derived from the Einstein model of the specific heat, that the temperature at which C_p/T^3 occurs is exactly $T_{max} = \Theta_E/5$. Hence, the obtained Einstein temperature is Θ_E = 96 K and Θ_E = 91 K for $SrCo_2Al_9$ and $BaCo_2Al_9$, respectively. Both values are in good agreement with previously refined values from the whole temperature fit.

Temperature dependence of a normalized resistivity (R/R_{300}) for $SrCo_2Al_9$ (blue line) and $BaCo_2Al_9$ (green line) is presented in Fig. 5. For both compounds the resistivity has a metallic-like character with the residual ratio RRR = R(300K)/R(1.9K) ≈ 6 and 10 for $SrCo_2Al_9$ and $BaCo_2Al_9$, respectively. There is no transition to the superconducting state observed above 1.8 K.

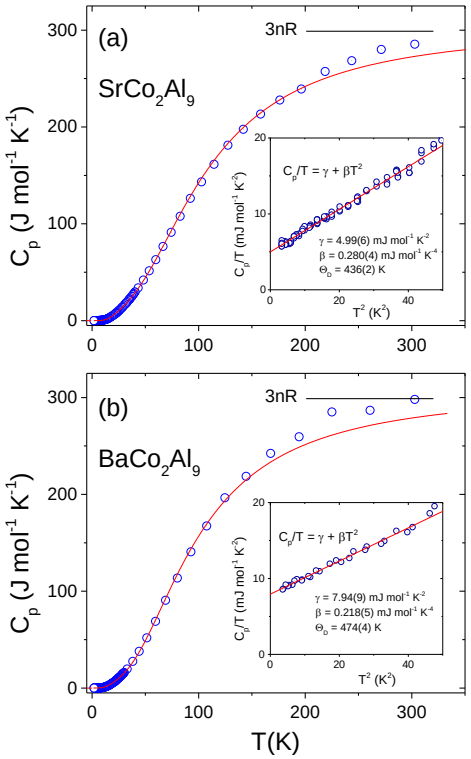

Figure 3 Heat capacity for a) $SrCo_2Al_9$ and b) $BaCo_2Al_9$. Main panel: overall temperature dependence of heat capacity. Inset: Low temperature data fitted with linear function.

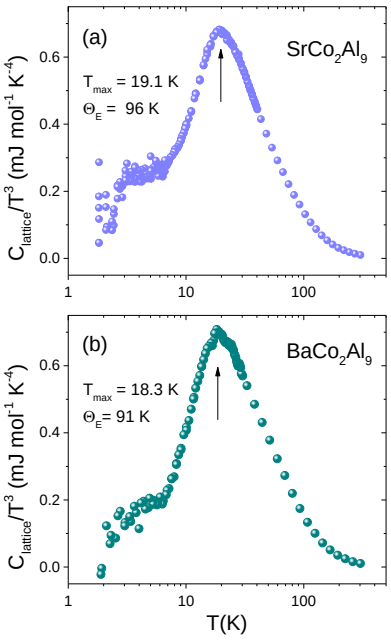

Figure 4 Temperature dependence of $C_{lattice}/T^3$ for $SrCo_2Al_9$ a) and $BaCo_2Al_9$ b).

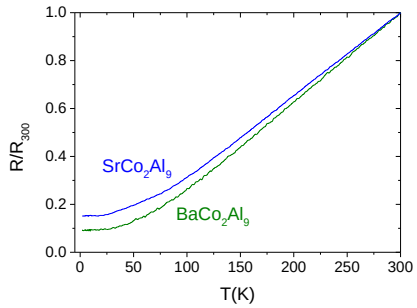

Figure 5 Normalized resistance vs. temperature for $SrCo_2Al_9$ (blue solid line) and $BaCo_2Al_9$ (green solid line).

Magnetoresistance defined as:

$$MR = \frac{R(B)-R_0}{R_0} \cdot 100\%,$$

where R(B) is the resistance in given field and R_0 is resistance without applied magnetic field, shown in Fig. 6 a) and b) is positive and at low fields has an ordinary parabolic character in both compounds. At higher fields the MR slowly saturates.

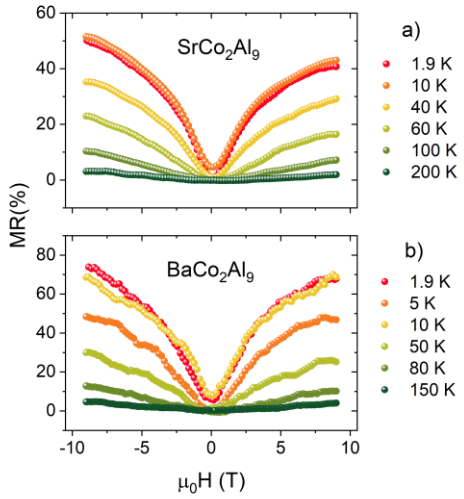

Figure 6 Magnetoresistance for a) $SrCo_2Al_9$ and b) $BaCo_2Al_9$. A slight asymmetry of the MR with respect to the field observed in the Sr compound results from a Hall contribution due to an imperfect linear 4-probe geometry. Data were smoothed using a moving average filter in order to improve readability.

At 1.9 K and 9 T the MR gains the values of approximately 40-50% and 60% for $SrCo_2Al_9$ and $BaCo_2Al_9$, respectively.

Electronic structure calculations were performed to gain insight into the observed difference between the electronic heat capacity coefficient in the Sr- and Ba-bearing compound.

Relaxed lattice constants and atomic positions (Tab. 2) are in a good agreement with experimental values (see Tab. 1 and ref. [16])..

Tab. 2 BFGS-relaxed cell parameters and atomic positions. Wyckoff symbols of atomic positions are given in parentheses. The only free parameter (not fixed by symmetry) is *x* of Al2.

	$SrCo_2Al_9$	$BaCo_2Al_9$
$a = b$	7.9035	7.9153
c	3.8985	3.9534
Ba/Sr (1*a*) $x = y = z$	0	
Al1 (3*f*) $x = z$ y	0 ½	
Al2 (6*m*) x $y = 2x$ z	0.2142 0.4284 ½	0.2158 0.4316 ½
Co (2*c*) x y z	0 1/3 2/3	

The band structure of $SrCo_2Al_9$, as presented in the Materials Project database [34,35], is rather complicated due to the large number of atoms in the primitive cell. The projected density of states of $SrCo_2Al_9$ and $BaCo_2Al_9$ (Fig. 7) show that in both cases the transition metal *d* states are completely filled, and the majority of DOS(E_F) is contributed by Al. Most of the Ba contribution lie above the Fermi level (ca. 0.5 to 3 eV), in accordance with an electron transfer from Ba/Sr to the Co_2Al_9 network. The inclusion of spin-orbit coupling (fully relativistic – FR) does not strongly affect the DOS in the -5 to 2 eV energy window, which is not surprising as the main contributions come from low-*Z* elements – Al and Co. Calculations of DOS for $SrCo_2Al_9$ was therefore performed only in the scalar-relativistic approach.

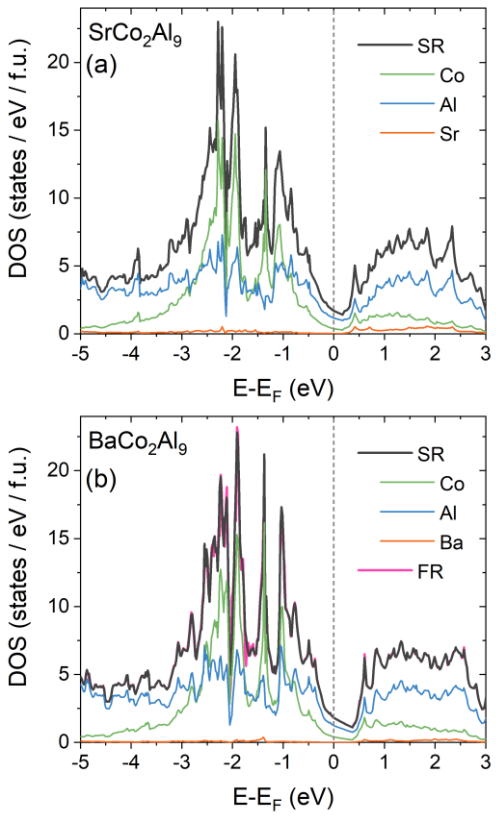

Figure 7 Density of states for $SrCo_2Al_9$ (a) and $BaCo_2Al_9$ (b). In the latter the DOS calculated within scalar- (SR, black line) and fully-relativistic (FR - including spin-orbit coupling, pink line) approach is compared. Green, blue, and orange lines show element-projected DOS contributions of Co, Al, and Sr/Ba, respectively, for the scalar-relativistic case.

As it is often observed in endohedral cluster compounds, the Fermi level lies in the vicinity of a pseudogap [15]. Interestingly, the difference in calculated DOS(E_F) between the two compounds is not large enough to explain the almost twofold difference between the Sommerfeld coefficient estimated from heat capacity measurements. Since γ is renormalized by electron-phonon interactions, one may expect much stronger electron-phonon coupling in $BaCo_2Al_9$, which should also lead to higher superconducting (SC) critical temperature T_c. However, as most of endohedral Al superconductors show T_c in the sub-2 K range [5–8,31,36,37] the lack of SC transition in the T = 1.8-300 K range is not surprising.

IV Conclusions

We have successfully synthesized single crystals of $SrCo_2Al_9$ and $BaCo_2Al_9$. Powder x-ray diffraction of crushed crystals confirms the hexagonal structure of $BaFe_2Al_9$-type with space group of *P6/mmm*. The crystals were studied with heat capacity and electrical transport measurements. Neither heat capacity nor resistivity measurements reveal any phase transition down to 1.8 K. Resistivity character of $SrCo_2Al_9$ and $BaCo_2Al_9$ is metallic and their magnetoresistance at T = 1.9 K has the value of 50% and 60% at 9 T, respectively. Low temperature heat capacity measurements give almost twice larger Sommerfeld coefficient for $BaCo_2Al_9$ (γ = 7.94(9) mJ mol^{-1} K^{-2}) than for $SrCo_2Al_9$ (γ = 4.99(6) mJ mol^{-1} K^{-2}). Electronic structure calculations show

Acknowledgements

The research at GUT was supported by the National Science Centre (Poland) grant (UMO-2018/29/N/ST5/01286).

References

[1] V.M.T. Thiede, W. Jeitschko, S. Niemann, T. Ebel, $EuTa_2Al_{20}$, $Ca_6W_4Al_{43}$ and other compounds with $CeCr_2Al_{20}$ and $Ho_6Mo_4Al_{43}$ type structures and some magnetic properties of these compounds, J. Alloys Compd. 267 (1998) 23–31.

[2] S. Niemann, W. Jeitschko, Ternary Aluminides AT_2Al_{20} (A = Rare Earth Elements and Uranium; T = Ti, Nb, Ta, Mo, and W) with $CeCr_2Al_20$-Type Structure, J. Solid State Chem. 114 (1995) 337–341.

[3] B. Fehrmann, W. Jeitschko, The intermetallic compounds $GdRe_2Al_{10}$ and $TbRe_2Al_{10}$, crystallizing with a stacking variant of the $YbFe_2Al_{10}$ type structure, Z. Naturforschung Sect. B- J. Chem. Sci. 54 (1999) 1277–1282.

[4] B. Fehrmann, W. Jeitschko, Lanthanoid Rhenium Aluminides with a High Content of Aluminum: $LnRe_2Al_{10}$ (Ln = Ho−Lu) with a New Structure Type and $NdRe_2Al_{10}$ with $CaCr_2Al_{10}$-Type Structure, Inorg. Chem. 38 (1999) 3344–3351.

[5] A. Sakai, K. Kuga, S. Nakatsuji, Superconductivity in the Ferroquadrupolar State in the Quadrupolar Kondo Lattice $PrTi_2Al_{20}$, J. Phys. Soc. Jpn. 81 (2012) 083702.

[6] M. Tsujimoto, Y. Matsumoto, T. Tomita, A. Sakai, S. Nakatsuji, Heavy-Fermion Superconductivity in the Quadrupole Ordered State of PrV_2Al_{20}, Phys. Rev. Lett. 113 (2014) 267001.

[7] M.J. Winiarski, B. Wiendlocha, M. Sternik, P. Wiśniewski, J.R. O'Brien, D. Kaczorowski, T. Klimczuk, Rattling-enhanced superconductivity in MV_2Al_{20} (M = Sc, Lu, Y) intermetallic cage compounds, Phys. Rev. B. 93 (2016) 134507.
[8] A. Yamada, R. Higashinaka, T.D. Matsuda, Y. Aoki, Superconductivity in Cage Compounds $LaTr_2Al_{20}$ with Tr = Ti, V, Nb, and Ta, J. Phys. Soc. Jpn. 87 (2018) 033707.
[9] R. Higashinaka, T. Maruyama, A. Nakama, R. Miyazaki, Y. Aoki, H. Sato, Unusual Field-Insensitive Phase Transition and Kondo Behavior in $SmTi_2Al_{20}$, J. Phys. Soc. Jpn. 80 (2011) 093703.
[10] A.S. Sefat, S.L. Bud'ko, P.C. Canfield, Properties of RRe_2Al_{10} (R=Y, Gd–Lu) crystals, Phys. Rev. B. 79 (2009) 174429.
[11] X. Zhang, W. Yi, K. Feng, D. Wu, Y. Yang, P. Zheng, J. Yao, Y. Matsushita, A. Sato, H. Jiang, H. Wang, Y. Shi, K. Yamaura, N. Wang, Crystal Growth, Structural, Electrical, and Magnetic Properties of Mixed-Valent Compounds $YbOs_2Al_{10}$ and $LuOs_2Al_{10}$, Inorg. Chem. 53 (2014) 4387–4393.
[12] P. Wiśniewski, P. Swatek, A. Gukasov, D. Kaczorowski, Ferromagnetism in UMn_2Al_{20} studied with polarized neutron diffraction and bulk magnetic measurements, Phys. Rev. B. 86 (2012) 054438.
[13] P. Swatek, D. Kaczorowski, Magnetic properties of $EuCr_2Al_{20}$, J. Magn. Magn. Mater. 416 (2016) 348–352.
[14] K. Fushiya, R. Miyazaki, R. Higashinaka, T.D. Matsuda, Y. Aoki, Single Crystal Growth and Anisotropic Magnetic Properties of Peanut-Shaped Cage Compound $Tm_6Cr_4Al_{43}$, Journal of the Physical Society of Japan, 2014.
[15] W. Xie, H. Luo, B.F. Phelan, T. Klimczuk, F.A. Cevallos, R.J. Cava, Endohedral gallide cluster superconductors and superconductivity in $ReGa_5$, Proc. Natl. Acad. Sci. 112 (2015) E7048–E7054.
[16] K. Turban, H. Schäfer, Zur kenntnis des $BaFe_2Al_9$-strukturtyps: Ternäre aluminide AT_2Al_9 mit A = Ba, Sr und T = Fe, Co, Ni, J. Common Met. 40 (1975) 91–96.
[17] V.M.T. Thiede, W. Jeitschko, Crystal Structure Of Europium Cobalt Aluminide (1/2/9), $EuCo_2Al_9$, Z. Für Krist. - New Cryst. Struct. 214 (2014) 149–150.
[18] X.-W. Lei, G.-H. Zhong, L.-H. Li, C.-L. Hu, M.-J. Li, J.-G. Mao, $Eu_3Co_2In_{15}$ and KM_2In_9 (M = Co, Ni): 3D Frameworks Based on Transition Metal Centered In9 Clusters, Inorg. Chem. 48 (2009) 2526–2533.
[19] N.P. Calta, F. Han, M.G. Kanatzidis, Synthesis, Structure, and Rigid Unit Mode-like Anisotropic Thermal Expansion of $BaIr_2In_9$, Inorg. Chem. 54 (2015) 8794–8799.
[20] K. Momma, F. Izumi, VESTA 3 for three-dimensional visualization of crystal, volumetric and morphology data, J. Appl. Crystallogr. 44 (2011) 1272–1276.
[21] W. Tremel, R. Hoffmann, Square nets of main-group elements in solid-state materials, J. Am. Chem. Soc. 109 (1987) 124–140.
[22] P.C. Canfield, T. Kong, U.S. Kaluarachchi, N.H. Jo, Use of frit-disc crucibles for routine and exploratory solution growth of single crystalline samples, Philos. Mag. 96 (2016) 84–92.
[23] A. LeBail, Whole powder pattern decomposition methods and applications: A retrospection, Powder Diffr. 20 (2005) 316–326.
[24] P. Giannozzi, S. Baroni, N. Bonini, M. Calandra, R. Car, C. Cavazzoni, Davide Ceresoli, G.L. Chiarotti, M. Cococcioni, I. Dabo, A.D. Corso, S. de Gironcoli, S. Fabris, G. Fratesi, R. Gebauer, U. Gerstmann, C. Gougoussis, Anton Kokalj, M. Lazzeri, L. Martin-Samos, N. Marzari, F. Mauri, R. Mazzarello, Stefano Paolini, A. Pasquarello, L. Paulatto, C. Sbraccia, S. Scandolo, G. Sclauzero, A.P. Seitsonen, A. Smogunov, P. Umari, R.M. Wentzcovitch, QUANTUM ESPRESSO: a modular and open-source software project for quantum simulations of materials, J. Phys. Condens. Matter. 21 (2009) 395502.
[25] J.P. Perdew, K. Burke, M. Ernzerhof, Generalized Gradient Approximation Made Simple, Phys. Rev. Lett. 77 (1996) 3865–3868.
[26] A.M. Rappe, K.M. Rabe, E. Kaxiras, J.D. Joannopoulos, Optimized pseudopotentials, Phys. Rev. B. 41 (1990) 1227–1230.
[27] P. Wilkes, Solid State Theory in Metallurgy, CUP Archive, 1973.
[28] M.J. Winiarski, T. Klimczuk, Crystal structure and low-energy Einstein mode in ErV_2Al_{20} intermetallic cage compound, J. Solid State Chem. 245 (2017) 10-16.
[29] M.J. Winiarski, T. Klimczuk, Synthesis and properties of HoT_2Al_{20} (T = Ti, V, Cr) intermetallic cage compounds, Intermetallics 85 (2017) 103-109.
[30] M.J. Winiarski, J.-C. Griveau, E. Colineau, K. Wochowski, P. Wiśniewski, D. Kaczorowski, R. Caciuffo, T. Klimczuk, Synthesis and properties of $A_xV_2Al_{20}$ (A = Th, U, Np, Pu) ternary actinide aluminides, J. Alloys Compd. 696 (2017) 1113-1119.
[31] Z. Hiroi, A. Onosaka, Y. Okamoto, J. Yamaura, H. Harima, Rattling and Superconducting Properties of the Cage Compound $Ga_xV_2Al_{20}$, J. Phys. Soc. Jpn 81 (2012) 124707.
[32] M.M. Koza, H. Mutka, Y. Okamoto, J. Yamaura, Z. Hiroi, On the microscopic dynamics of the 'Einstein solids' AlV_2Al_{20} and GaV_2Al_{20}, and of YV_2Al_{20}: a benchmark system for 'rattling' excitations, Phys. Chem. Chem. Phys. 17 (2015), 24837-24850.

[33] M.M. Koza, A. Leithe-Jasper, E. Sischka, W. Schnelle, H. Borrmann, H. Mutka, Y. Grin, Effect of the electropositive elements A = Sc, La, and Ce on the microscopic dynamics of AV_2Al_{20}, Phys. Chem. Chem. Phys. 16 (2014) 27119-27133.
[34] A. Jain, S.P. Ong, G. Hautier, W. Chen, W.D. Richards, S. Dacek, S. Cholia, D. Gunter, D. Skinner, G. Ceder, K.A. Persson, Commentary: The Materials Project: A materials genome approach to accelerating materials innovation, APL Mater. 1 (2013) 011002.
[35] K. Persson, Materials Data on $SrAl_9Co_2$ (SG:191) by Materials Project, (2014).
[36] D.C. Peets, E. Cheng, T. Ying, M. Kriener, X. Shen, S. Li, D. Feng, Type-I superconductivity in Al_6Re, Phys. Rev. B. 99 (2019) 144519.
[37] T. Klimczuk, M. Szlawska, D. Kaczorowski, J.R. O'Brien, D.J. Safarik, Superconductivity in the Einstein solid $VAl_{10.1}$, J. Phys. Condens. Matter. 24 (2012) 365701.